PLOS ONE

RESEARCH ARTICLE

Predicting saturated and near-saturated hydraulic conductivity using artificial neural networks and multiple linear regression in calcareous soils

Hasan Mozaffari[1], **Ali Akbar Moosavi**[1]*, **Mohammad Amin Nematollahi**[2]*

1 Department of Soil Science, College of Agriculture, Shiraz University, Shiraz, Iran, **2** Department of Biosystems Engineering, College of Agriculture, Shiraz University, Shiraz, Iran

* aamousavi@gmail.com, aamousavi@shirazu.ac.ir (AAM); manemat54@gmail.com (MAN)

Citation: Mozaffari H, Moosavi AA, Nematollahi MA (2024) Predicting saturated and near-saturated hydraulic conductivity using artificial neural networks and multiple linear regression in calcareous soils. PLoS ONE 19(1): e0296933. https://doi.org/10.1371/journal.pone.0296933

Editor: A. L. Mahfoodh, UNITEN: Universiti Tenaga Nasional, MALAYSIA

Received: October 2, 2023

Accepted: December 15, 2023

Published: January 10, 2024

Data Availability Statement: All relevant data are within the manuscript and its Supporting Information files.

Funding: This research was supported by Shiraz University.

Competing interests: There is no competing interest.

Abbreviations: ANNs, Artificial neural networks; BD, Bulk density; Ca^{2}-+, Water-soluble calcium; CCE, Calcium carbonate equivalent (lime); CV,

Abstract

Hydraulic conductivity (K_ψ) is one of the most important soil properties that influences water and chemical movement within the soil and is a vital factor in various management practices, like drainage, irrigation, erosion control, and flood protection. Therefore, it is an essential component in soil monitoring and managerial practices. The importance of K_ψ in soil-water relationship, difficulties for its measurement in the field, and its high variability led us to evaluate the potential of stepwise multiple linear regression (SMLR), and multilayer perceptron (MLPNNs) and radial-basis function (RBFNNs) neural networks approaches to predict K_ψ at tensions of 15, 10, 5, and 0 cm (K_{15}, K_{10}, K_5, and K_0, respectively) using easily measurable attributes in calcareous soils. A total of 102 intact (by stainless steel rings) and composite (using spade from 0–20 cm depth) soil samples were collected from different land uses of Fars Province, Iran. The common physico-chemical attributes were determined by the common standard laboratory approaches. Additionally, the mentioned hydraulic attributes were measured using a tension-disc infiltrometer (with a 10 cm radius) in situ. Results revealed that the most of studied soil structure-related parameters (soil organic matter, soluble sodium, sodium adsorption ratio, mean weight diameter of aggregates, pH, and bulk density) are more correlated with K_5 and K_0 than particle-size distribution-related parameters (sand, silt, and standard deviation and geometric mean diameter of particles size). For K_{15} and K_{10}, the opposite results were obtained. The applied approaches predicted K_{15}, K_{10}, K_5, and K_0 with determination coefficient of validation data (R^2_{val}) of 0.52 to 0.63 for SMLR; 0.71 to 0.82 for MLPNNs; and 0.58 to 0.78 for RBFNNs. In general, the capability of the applied methods for predicting K_ψ at all the applied tensions was ranked as MLPNNs > RBFNNs > SMLR. Although the SMLR method provided easy to use pedotransfer functions for predicting K_ψ in calcareous soils, the present study suggests using the MLPNNs approach due to its high capability for generating accurate predictions.

Coefficient of variations; D, Fractal dimension of particle-size distribution; d_g, Geometric mean of particles size diameter; EC, Electrical conductivity of saturated extract; FFNNs, Feed-forward neural networks; K^+, Water-soluble potassium; K_ψ, Hydraulic conductivity at tension ψ; K_0, Hydraulic conductivity at tension 0 cm (saturated hydraulic conductivity); K_5, Hydraulic conductivity at tension 5 cm; K_{10}, Hydraulic conductivity at tension 10 cm; K_{15}, Hydraulic conductivity at tension 15 cm; KR, Kurtosis coefficient; KS, Statistic of Kolmogorov-Smirnov normality test; Mg^{2+}, Water-soluble magnesium; Max, Maximum; Min, Minimum; MLPNNs, Multilayer perceptron neural networks; MWD, Mean weight diameter of aggregates; n, Number of data; Na^+, Water-soluble sodium; NRMSE, Normalized root mean square error; NS, Nash-Sutcliffe coefficient; pH, pH of saturated paste; PSD, Particle-size distribution; PTF, Pedotransfer function; Q_ψ, Volume of water infiltrates into the soil per unit time at tension ψ; r, Radius of the disc infiltrometer apparatus; R, Pearson's correlation coefficient; R^2, Determination coefficient; RBFNNs, Radial-basis function neural networks; RPD, Residual prediction deviation; SAR, Sodium adsorption ratio; SK, Skewness coefficient; SMLR, Stepwise multiple linear regression; SOM, Soil organic matter; Subscript cal, Calibration subset; Subscript val, Validation subset; VC, Variability class according to Wilding's classification; α, Sorptive number; σ_g, Geometric standard deviation of particles size diameter; ψ, Applied tension.

Introduction

Increased population pressure and the necessity of efficient water management have recently led attentions to reuse arid and semiarid soils as potential productive soil resources [1]. Hydraulic conductivity (K_ψ) is an important attribute in designing and monitoring drainage and irrigation systems and to characterize many aspects of water flow within unsaturated soils such as irrigation, aquifer recharge, infiltration of rainfall and runoff, nutrient transportation, pollutants, and pesticides, and water balance [2–4]. There are some crucial factors such as pores size distribution and soil structure [5,6], bulk (apparent) density (BD) [7], particle-size distribution (PSD) [8], and soil organic matter, (SOM) content [9] that can significantly affect K_ψ.

The values of K_ψ are highly depending on the methods used for their determination [1]. Moreover, its measurement both in the field (by double rings, tension-disk infiltrometer, or Guelph permeameter) and laboratory (using the constant and falling head approaches) is a laborious, challenging, and costly process [10]. Consequently, various efforts have been made to indirectly determine saturated and, to a lesser extent, unsaturated or near-saturated hydraulic conductivity. This has been achieved through creation of pedotransfer functions (PTFs), which used easily measurable soil attributes. These easily measurable soil attributes include soil texture and PSD parameters, BD, mean weight diameter of aggregates (MWD), SOM content, calcium carbonate equivalent (CCE), and others. To estimate saturated and unsaturated hydraulic conductivity, different approaches have been used in literature like, linear [11–14] and non-linear [15,16] regressions, and different machine learning algorithms [13,16–19]. Nevertheless, the potential of PTFs to accurately predict K_ψ is limited due to not incorporating soil structure, which is a crucial factor influencing hydraulic conductivity [20].

Artificial neural networks (ANNs), ANNs-based PTFs, and other related approaches have been widely employed as powerful modeling tools in various fields of science and engineering [21–23]. The ANNs are inspired by the human brain which is able to simulate the complex relation between input and output data [24]. According to literature, ANNs typically exhibit higher efficiency and potentials to estimate hardly measurable soil attributes rather than conventional regression approaches [25–27]. There are some advantages of ANNs approaches compared to traditional PTFs. For instance, in the ANNs approaches there is: i) no need to pre-assumptions for modeling; ii) no need to priori assumptions of data distribution; iii) high capability to model complex and non-linear behaviors; and iv) high compatibility with missing and noisy data [24]. However, ANNs approaches in comparison to conventional PTFs have some weaknesses like: i) "black boxes" modeling; ii) necessity for a large number of data to obtain the optimal weights and biases of the network; and iii) necessity for trial and error approaches to select the most suitable parameters in their structures [28,29].

Two feed-forward NNs (FFNNs), including multilayer perceptron (MLPNNs) and radial-basis function (RBFNNs), have been commonly used among various types of ANNs as efficient tools for recognizing patterns or approximate functions [30,31].

Although ANNs have been used to predict saturated hydraulic conductivity (K_0) in several studies [32–37], there is a limitation in literature which applied ANNs to predict unsaturated hydraulic conductivity especially in calcareous soils. In this regard, Moosavi and Sepaskhah [38] in the Fars Province of Iran, found that the most accurate prediction of K_ψ at tensions of 20, 15, 10, 6, 3, and 0 cm were obtained with a four-layer MLPNNs with three nodes in the first and four nodes in the second hidden layers. Sihag [39] in sandy soils of India reported that the prediction of unsaturated hydraulic conductivity by back propagation algorithm based on ANNs approach works better than fuzzy logic. Jian et al. [40] in the USA soils found the two-hidden layers MLPNNs approach with the first and the second layers of five and three

nodes had a good performance to predict K_ψ at 2 cm tension when trained with soil texture components (i.e., clay, silt, and sand percentages).

In addition to the mentioned limitation, there are no reports about the prediction of field measured near-saturated K_ψ using multiple linear regression (MLR), MLPNNs, and RBFNNs approaches and comparing their modeling potential. Therefore, novel aspects of the present study were covering the potential of two common FFNNs to predict saturated and near-saturated K_ψ in calcareous soils and also comparing their capability with that of the MLR approach. In general, this study aimed to: i) predict K_ψ of calcareous soils at tensions of 15, 10, 5, and 0 cm using MLPNNs and RBFNNs along with MLR, and ii) compare capability of the mentioned approaches and their accuracies to predict K_ψ in calcareous soils.

Materials and methods

Study area

Totally 102 locations were randomly selected in the Fars Province, Iran to measure physico-chemical and hydraulic attributes of the soils, which cover the most relevant land uses and soil types. It should be noted that for developing reliable models to predict specific soils attribute, the number of input data, which is largely depends on difficulties and costs for its determining, is very important. For this purpose, normally the 100 data are trustworthy and appropriate in soil science studies. Of course, higher numbers of input data result in more reliable models. Still, due to difficulties and spending lots of time for measuring the K_ψ, the 102 data would be appropriate for performing the present study. In addition, the random selection of experimental points while considering different land uses can help to include almost all soil types with different hydraulic, physical, and chemical attributes in the study. Therefore, the obtained results can be used in larger areas with similar soil conditions.

General descriptions of the study region (Fars Province) and the soils were summed up in Table 1. The Fars Province, in south and southwest regions of Iran, has a great potential to grow many types of agricultural plants like wheat, barley, corn, rice, alfalfa, etc. On the other hand, there are different types of land uses, like croplands, pasture, garden, woodland, etc. in the mentioned Province. The soils of Fars Province are calcareous and relatively calcareous (with a CCE contents of 12.5–70.6% based on our data in the present study), which can be a

Table 1. General descriptions of the study region and the studied soils.

Characteristic	Description	References
Location	Fars Province	-
Geographical coordinates	50˚ 30′ to 55˚ 38′ E and 27˚ 03′ to 31˚ 42′ N	-
General climate	Arid and semi-arid	-
Climate regime based on Köppen-Geiger	BWh, BSk, BSh	[41]
Mean annual temperature	17.5˚C	[42]
Annual precipitation	5 to 100 cm	[43]
Elevation from the mean sea level	0.5 to 4 km	[44]
Soil moisture regimes	Xeric, ustic, aridic	[45]
Soil temperature regimes	Mesic, thermic, hyperthermic	[45]
Parent material	Soluble dolomite and calcite limestone	[46]
Studied soil types according to Taxonomy classification	Inceptisols (71 soils), Aridisols (18 soils), and Entisols (13 soils)	[44,47]
Studied land uses	Croplands (wheat, barley, corn, rice, and fallow), pasture, woodland (oak forests)	-

https://doi.org/10.1371/journal.pone.0296933.t001

good representative for calcareous soils in the Middle East. Due to these mentioned reasons, the Fars Province was selected as target area for performing the present study.

At each of the 102 selected locations, water infiltration was measured using a tension-disk infiltrometer apparatus. Intact soil samples of 3.5 cm diameter and 2 cm height (using stainless steel rings) and 1 kg composite samples (using spade) were taken from the depth of 0 to 20 cm to measure soil physico-chemical attributes.

Analyzing selected physico-chemical attributes of the soils

Air-dried soil samples, that were ground and sieved to sizes of 8 and 2 mm, were prepared to determine the selected physico-chemical attributes using standard laboratory procedures. Generally, in the present study the selected physico-chemical attributes were divided in two groups: i) PSD-related parameters, and ii) structure-related parameters. The PSD-related parameters contain sand, silt, clay, geometric mean (d_g) and geometric standard deviation (σ_g) of particles size diameter, and fractal dimension (D). The PSD and its related parameters affect pores size distribution due to the sizes of primary particles. For instance, water infiltrates faster in the coarse-textured soils compared with the fine-textured soils due to having a high content of sand. On the other hand, existing clay content in soil is very essential for aggregation. Therefore, the PSD-related attributes may have significant effects on hydraulic parameters, like K_ψ. Subsequently, the structure-related parameters contain BD, MWD, pH, SOM, CCE, electrical conductivity (EC), water-soluble sodium (Na^+), potassium (K^+), calcium (Ca^{2+}), and magnesium (Mg^{2+}), and sodium adsorption ratio (SAR). In general, the mentioned structure-related parameters may affect the pores size distribution of soils, due to their effects on aggregation and disaggregation. The K_ψ values may therefore be affected by these structure-related parameters.

The soil PSD and texture were determined using the combined sedimentation (hydrometer) and wet-sieving methods [48]. More specifically, the PSD of the soils was obtained based on measuring the density of soil-water suspension at 120, 300, and 600 sec, and at 1, 3, 6, and 24 h by hydrometer (for particles of less than 0.05 mm diameter) and remaining particles on sieves with opening diameters of 1, 0.5, 0.15, and 0.05 mm (for sand fraction) [48].

The BD of soils was measured using stainless steel rings with 3.5 cm diameter and 2 cm height [49]; MWD using a series of 8 sieves with opening diameters of 4, 2, 1, 0.8, 0.6, 0.4, 0.2, and 0.075 mm by dry-sieving method [50]; pH of saturated paste using pH-meter (glass electrode) [51]; SOM content using oxidation of soil organic carbon by potassium dichromate and titration with ammonium ferro sulfate as reductant (Walkley-Black wet oxidation) method [52]; CCE using back titration with hydrochloric acid (HCl) method [53]; EC of saturated extract using conductometer (EC-meter) [54]; water-soluble Na^+ and K^+ of saturated extract using a flame photometer [55]; and water-soluble Ca^{2+} and Mg^{2+} of saturated extract using titration with EDTA method [56].

In addition, the PSD data was used to calculate some indices like, d_g and σ_g [57], and D [58]. Furthermore, SAR was calculated using the values of water-soluble Na^+, Ca^{2+}, and Mg^{2+} (for details see Mozaffari et al., [59]).

Infiltration experiments

A single-disc tension infiltrometer with 10 cm radius was used to conduct the infiltration experiments (Fig 1). At first, at each experimental location, the residues of the plant materials were gently eliminated from the soil surface without causing any alteration to the soil structure. To ensure a suitable hydraulic connection between the soil surface and the disc membrane of the infiltrometer, we used a thin contact layer (nearly 0.5 cm) of fine sand with

Fig 1. Measurement of K_ψ by tension-disk infiltrometer at different land uses.

https://doi.org/10.1371/journal.pone.0296933.g001

particle diameters of 0.1 to 0.25 mm. Fresh water (with EC of 0.6 dS m^{-1} and SAR of 0.5 $meq^{0.5}$ $L^{-0.5}$) was used to fill the device reservoir for conducting the infiltration experiments. After that, the infiltrometer was gently put onto the layer of sand and fixed. The experiment was started with the intended maximum tension, which was considered as 15 cm during this study. The Mariotte tubes and air tower were used for setting the applied tensions. In the present study, for performing infiltration test, four successive tensions including 15, 10, 5, and 0 cm were applied at each experimental site. At each tension, the height of infiltrated water was manually recorded at the time intervals of 0.25 min (for the first 5 min) and 1 min to reach the steady-state conditions. Consider that, the steady-state conditions are achieved when at least five successive infiltration rates became similar [60]. The time needed to reach the steady state conditions varies for different soils, and usually falls between 20 to 60 min at each applied tension.

Calculating near-saturated and saturated hydraulic conductivity (K_ψ)

The K_ψ at different applied tensions (ψ) was calculated using the method introduced by Ankeny et al. [61]. According to their theory, the K_ψ was determined based on the collected infiltration data using well-known Wooding's approach [62]. In this particular approach, it is

assumed that the variation of K_ψ with respect to ψ (as described in Eq 1) follows an exponential pattern. This assumption holds true when water enters the soil from a circular source with a fixed radius "r" under a constant tension [62–64]:

$$K_\psi = K_0 \exp(\alpha\, \psi) \tag{1}$$

where K_0 and α are hydraulic conductivity ($L\ T^{-1}$) at zero cm ψ and the sorptive number (L^{-1}), respectively [65,66]. Wooding [62] derived the subsequent analytical solution:

$$Q_\psi = \pi\, r^2\, K_\psi + \frac{4\,\pi\, r^2\, K_\psi}{\pi\, r\, \alpha} = \pi\, r^2\, K_\psi \left(1 + \frac{4}{\pi\, r\, \alpha}\right) \tag{2}$$

where Q_ψ represents the volume (L^3) of water infiltrates into the soil per unit time (T), at tension ψ under steady-state conditions and r denotes radius (L) of the disc infiltrometer apparatus.

Based on Ankeny et al. [61] analysis, by applying Wooding's solution for unsaturated steady-state conditions and substituting K_ψ with Eq (1), as well as replacing ψ_i and ψ_{i1+} into the resulting equation, we would obtain Eqs (3) and (4).

$$Q_{\psi_i} = \pi\, r^2\, K_0 \exp(\alpha\, \psi_i) + \frac{4\,\pi\, r^2\, K_0 \exp(\alpha\, \psi_i)}{\pi\, r\, \alpha} \tag{3}$$

$$Q_{\psi_{i+1}} = \pi\, r^2\, K_0 \exp(\alpha\, \psi_{i+1}) + \frac{4\,\pi\, r^2\, K_0 \exp(\alpha\, \psi_{i+1})}{\pi\, r\, \alpha} \tag{4}$$

Ankeny et al. [61] solved Eqs (3) and (4) simultaneously as follows:

$$K_{\psi_i(1)} = \frac{Q_{\psi_i}}{\pi\, r^2 + 2\,\Delta\psi\, r\left(\frac{Q_{\psi_i} + Q_{\psi_{i+1}}}{Q_{\psi_i}}\right) / \left(\frac{Q_{\psi_i} - Q_{\psi_{i+1}}}{Q_{\psi_i}}\right)} \tag{5}$$

$$K_{\psi_i(2)} = \frac{Q_{\psi_{i+1}} K_{\psi_i(1)}}{Q_{\psi_i}} \tag{6}$$

In present study, the values of 0 and 5, 5 and 10, and 10 and 15 cm tensions were used to solve three equations simultaneously. Ankeny et al. [61] stated that the arithmetic average value has the best compatibility with the K_ψ, where K_{ψ_i} is obtained from the (ψ_i, ψ_{i+1}) rate pair ($K_{\psi_i} = \frac{K_{\psi_{i+1}} + K_{\psi_i}}{2}$). Eqs (7) to (10) indicate how K_0, K_5, K_{10}, and K_{15} were practically calculated [61]:

$$K_0 = K_{0(0,5)} \tag{7}$$

$$K_5 = \frac{K_{5(0,5)} + K_{5(5,10)}}{2} \tag{8}$$

$$K_{10} = \frac{K_{10(5,10)} + K_{10(10,15)}}{2} \tag{9}$$

$$K_{15} = K_{15(10,15)} \tag{10}$$

Stepwise multiple linear regression (SMLR)

The SMLR, which still is one of the most commonly used and standardized approaches for developing PTFs [20], was employed for predicting K_ψ as described below:

$$K_\psi = a_0 + a_1\ V_1 + a_2 V_2 + \ldots + a_N\ V_N \tag{11}$$

where V_1 to V_N are the independent variables (easily measurable soil attributes), a_0 to a_N denote regression coefficients, and N shows the number of independent variables. The significant predictor variables were selected using a forward approach. For developing SMLR-PTFs, the K_ψ at different applied tensions and easily measurable soil attributes were selected as dependent and independent variables, respectively. The STATISTICA (version 8.0) software package was used for developing SMLR-PTFs.

Artificial neural networks (ANNs)

Multilayer perceptron NNs (MLPNNs). The ANNs are a subset of machine learning, which consist of several layers and processing elements called neurons. Two unknown parameters including weights (w_{ji}) and biases (b_j) in the structure of the MLPNNs should be adjusted by the training process [24,67]. For this purpose, an error function, which is a function of weights and biases, should be minimized as follows:

$$E = \sum_{i=1}^{m}\sum_{j=1}^{n}\left(P_{ij} - O_{ij}\right)^2 \tag{12}$$

where O_{ij} and P_{ij} denote the observed (measured) and predicted values of dependent variable, respectively. m and n are the number of output and data fed into the networks, respectively. An iterative back-propagation algorithm is usually used to adjust the w_{ji} as following:

$$w_{ji}(k+1) = w_{ji}(k) + \Delta w_{ji}(k) \tag{13}$$

A generalized delta-learning rule is applied to determine the $\Delta w_{ji}\,(k)$ values [24,67].

In the current study, for training MLPNNs, various hidden layers of different numbers of nodes (neurons) were examined. The MATLAB software package was used to select the most effective hidden layers combination and their number of neurons, and to predict the K_ψ. For training the MLPNNs, an architecture with two hidden layers were selected for all K_ψ that includes 8 and 12, 6 and 11, 7 and 10, and 9 and 14 neurons in the first and second layers to estimate the K_0, K_5, K_{10}, and K_{15}, respectively.

Different transfer functions and learning (training) algorithms were tested in the mentioned MLPNNs to achieve the lowest value of Eq (12). The Levenberg-Marquardt algorithm was employed as learning (training) algorithm in the structure of the used MLPNNs for estimating all K_ψ. In addition, the sigmoid transfer function was used in the hidden layer, whereas linear transfer function was employed for the output (target) layer.

Radial-basis function NNs (RBFNNs). The RBFNNs is another type of FFNNs that composed of two layers with simple structure and fast in learning. There are two main stages for learning process in RBFNNs: i) obtaining the centers of the clustered input variables (data) by the unsupervised approaches [24,67,68], and ii) determining the weights of the network using the least square approach. The RBFNNs output is computed as:

$$Y_q(X) = \sum_{K_\psi=1}^{\varepsilon} w_{qj}\ \varphi_j(\|X - U_j\|) + b_q \tag{14}$$

where X and U_j show the input vector and the vector corresponding to the center of the RBF φ_j (as transfer function), respectively. The Gaussian function is commonly employed as a basis function for the RBFNNs, which is given as:

$$\varphi_j\left(\|X-U_j\|\right)=\exp\left(-\frac{|X-U_j|}{2\,\sigma^2}\right) \tag{15}$$

where σ denote the spread of the RBF.

Data analysis

At first, the selected hydraulic, physical, and chemical attributes were subjected to calculate the descriptive statistics and normality test using Excel (version 2019) and SPSS (version 26) software packages. Attributes that did not follow normal distribution were transformed using the natural logarithm (ln) transformation to be closer to the normal distribution. To evaluate the potential of selected modeling approaches to predict K_ψ at different applied tensions by easily measurable soil attributes, the total of 102 laboratory/field measured soil attributes were randomly divided to 75% and 25% of the dataset as the calibration and validation subsets, respectively [38,69–71]. Furthermore, in order to ensure that: i) both validation and calibration subsets of K_ψ have approximately the same distributions, and ii) the mean values of the aforementioned subsets have no significant difference; the 1:1 line (using Excel software) and t-test analysis (using STATISTICA software) were used, respectively [72]. After that, the K_ψ values at different applied tensions (as dependent variables) and studied physico-chemical attributes (as independent variables) related to calibration subset were imported to the STATISTICA (version 8) software package for developing PTFs using forward-SMLR approach. The most significant and effective easily measurable attributes were appeared in four developed SMLR-PTFs to predict K_ψ at different applied tensions. To avoid the complexity of the NNs models, the appeared physico-chemical attributes in developed SMLR-PTFs were imported to MATLAB software package as independent variables for predicting K_ψ using MLPNNs and RBFNNs models. It is worth mentioning that, all applied models were developed by the calibration subset and then tested by the validation subset.

Statistical evaluation of the models

Several statistical indices including the determination coefficient (R^2), the Nash-Sutcliffe coefficient (NS), the residual prediction deviation (RPD), and the normalized root mean square error (NRMSE) were employed to assess and compare the performance of the models (Eqs 16 to 19):

$$R^2=\frac{\left(\sum_{i=1}^{n}(O_i-\bar{O})(P_i-\bar{P})\right)^2}{\sum_{i=1}^{n}(O_i-\bar{O})^2\sum_{i=1}^{n}(P_i-\bar{P})^2} \tag{16}$$

$$NS=1-\frac{\sum_{i=1}^{n}(O_i-P_i)^2}{\sum_{i=1}^{n}(O_i-\bar{O})^2} \tag{17}$$

$$RPD=\frac{Sd}{SEP} \tag{18}$$

Table 2. Different classifications for the selected performance criteria.

NRMSE†		NS††		RPD†††	
Range	**Classification**	**Range**	**Classification**	**Range**	**Classification**
0–10%	Excellent	0.90–1	Very good	≥ 2.5	Excellent
10–20%	Good	0.80–0.90	Good	2.0–2.5	Very good
20–30%	Fair	0.65–0.80	Acceptable	1.8–2.0	Good
$> 30\%$	Poor	< 0.65	Unsatisfactory	1.4–1.8	Fair
-	-	-	-	1.0-.1.4	Poor
-	-	-	-	< 1	Very poor

†: Normalized root mean square error (After Bannayan and Hoogenboom [73]).

††: The Nash-Sutcliffe coefficient (After Ritter and Muñoz-Carpena [74]).

†††: The residual prediction deviation (After Mouazen et al. [75]).

https://doi.org/10.1371/journal.pone.0296933.t002

$$\mathrm{NRMSE}(\%) = \frac{\sqrt{\sum_{i=1}^{n} \frac{(O_i - P_i)^2}{n}}}{\bar{O}} \times 100 \quad (19)$$

where P_i and O_i show the predicted and measured (observed) data, n is number of data, Sd and SEP denote the standard deviation and standard error of the measured data (SEP is equal to RMSE of the predicted data). Table 2 shows the reported classifications for different ranges of NRMSE, NS, and RPD performance criteria. The statistical calculations were performed using the MATLAB software package.

Results and discussion

Summary statistics

According to Fig 2, the soils included a broad range of textures (mainly silt loam and loam classes). Therefore, it can be expected that the PSD-related parameters (clay, silt, sand, d_g, σ_g, and D) be significant and effective parameters for predicting K_ψ. It should be noted that we used the United State Department of Agriculture (USDA) guideline to classify the soil texture components, which means that a particle with diameter of less than 0.002 mm is clay; with diameter of 0.002 to 0.05 mm is silt; and with diameter of 0.05 to 2 mm is sand [76]. The d_g, σ_g, and D are criteria of PSD data. They represent unique features of PSD. For example, with increasing clay content and decreasing sand content, the D values increase and the d_g values decrease [57,77], but their relationships with soil texture components (sand, silt, and clay contents) are not linear. While, the σ_g parameter depends on combination of all texture components in the soil [57]. The primary particles (sand, silt, and clay) contents affect pores size distribution due to their sizes and also their impacts on aggregation. Furthermore, macropores and mesopores play crucial roles in water flow through the soil, especially when it comes to processes such as infiltration and the rapid movement of water, solutes, and pollutants through the soil [78,79]. Therefore, the PSD-related parameters may affect infiltration rate and subsequently K_ψ at different tensions.

The obtained results demonstrated, among studied soil attributes, the D and SAR with coefficient of variations (CV) values of 2.1% and 277%, respectively, represent the lowest and the highest CVs (Table 3). According to classification proposed by Wilding [80], the D, BD, and pH belong to the class of low variability ($0\% < \mathrm{CV} \leq 15\%$); K_5, MWD, silt, σ_g, and CCE belong

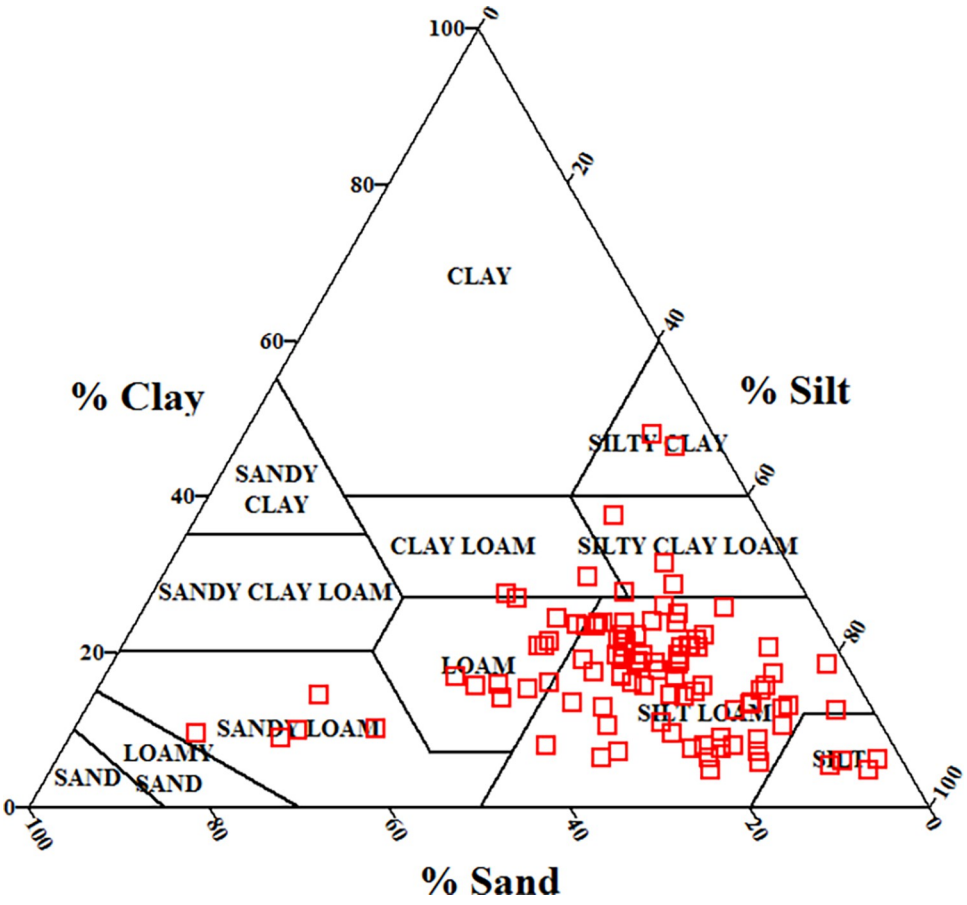

Fig 2. The United State Department of Agriculture (USDA) soil textural classes (n = 102).

https://doi.org/10.1371/journal.pone.0296933.g002

to the class of moderate variability (15% < CV ≤ 35%); and the remaining studied soil attributes belong to the class of high variability (CV > 35%). The higher CV values show the greater level of the data dispersion around the mean. Therefore, the high variability of an attribute in a dataset enables the researcher to model that parameter with higher certainty and the resulting model can be used on a larger scale. In contrast, a lower CV value of input data may result in a good model, while the applicability of the model is limited to a small range of target attribute. Of course, it should be noted that some attributes (for instance D, BD, and pH) inherently have low CVs due to the low values of standard deviation in comparison with their mean values. More specifically, the D value normally changes between 2.4 to 3 in soils, which in the present study varied between 2.56 to 2.85. Therefore, the minimum value of CV was obtained for this property. While, in arid and semi-arid regions, like the study area, very high values of EC and water-soluble cations can be observed. In irrigated fields with fresh water, the soluble salts and cations are leached toward the deeper sections of soil profile. While, in the pastures or rainfed fields, the soluble salts and cations of subsoil may migrate to the surface layers of soils through capillary movement and accumulate there. Therefore, the high variability of EC, water-soluble Na^+, K^+, Ca^{2+}, and Mg^{2+}, and SAR may be observed in such arid and semi-arid regions. In this regard, the EC values of 0.26 to 76.7 dS m^{-1} was reported by Mozaffari et al. [76] in the soils of Fars Province, Iran. In addition, moderate and high variabilities of K_ψ in the present study indicate that the obtained models may work well on a larger scale with similar soils.

Table 3. The descriptive statistics and related normality test parameters for the selected attributes of the studied soils (n = 102).

Property	Unit	Min	Max	Mean	CV (%)	VC	SK	KR	KS†
K_{15}	cm h^{-1}	0.084	1.17	0.520	39.5	High	0.604	0.727	0.070 ^{ns}
K_{10}	cm h^{-1}	0.097	1.81	0.877	36.1	High	0.350	0.361	0.039 ^{ns}
K_5	cm h^{-1}	0.790	3.68	2.17	27.4	Moderate	0.091	-0.726	0.075 ^{ns}
K_0	cm h^{-1}	1.44	10.9	5.72	41.3	High	0.159	-0.966	0.093 ^{ns}
MWD	mm	0.374	3.52	1.47	28.6	Moderate	1.10	4.68	0.064 ^{ns}
Sand	%	2.28	60.5	23.1	48.1	High	0.897	1.96	0.094 ^{ns}
Silt	%	13.6	91.0	59.4	23.7	Moderate	-0.395	0.927	0.061 ^{ns}
Clay	%	4.88	47.9	17.5	45.2	High	1.03	2.64	0.079 ^{ns}
d_g	μm	3.32	32.2	12.6	43.8	High	1.08	1.31	0.130 ^{ns}
σ_g	mm	2.50	12.2	6.20	27.7	Moderate	0.182	0.616	0.057 ^{ns}
D	-	2.56	2.85	2.71	2.10	Low	-0.637	0.326	0.108 ^{ns}
BD	g cm^{-3}	1.27	1.88	1.56	7.52	Low	0.359	0.619	0.077 ^{ns}
pH	-	6.60	7.99	7.47	3.56	Low	-0.836	0.968	0.112 ^{ns}
EC	dS m^{-1}	0.364	3.18	0.816	58.3	High	2.45	7.28	0.219 *
ln(EC)	-	-1.01	1.16	-0.317	-	-	1.06	0.958	0.129 ^{ns}
Na^+	mg L^{-1}	8.28	153	28.7	85.3	High	3.23	13.0	0.202 *
ln(Na^+)	-	2.11	5.03	3.14	-	-	0.590	0.392	0.061 ^{ns}
K^+	mg L^{-1}	1.66	75.2	19.6	92.3	High	1.42	1.12	0.176 *
ln(K^+)	-	0.507	4.32	2.58	-	-	0.170	-0.859	0.101 ^{ns}
Ca^{2+}	mg L^{-1}	68	720	181	66.5	High	2.58	7.29	0.222 *
ln(Ca^{2+})	-	4.22	6.58	5.06	-	-	1.08	1.18	0.097 ^{ns}
Mg^{2+}	mg L^{-1}	4.80	60.0	12.5	100	High	2.23	4.41	0.225 *
ln(Mg^{2+})	-	1.57	4.09	2.21	-	-	1.08	0.158	0.132 ^{ns}
SAR	(meq L^{-1})$^{0.5}$	0.185	34.1	2.01	277	High	4.68	22.88	0.404 *
ln(SAR)	-	-1.69	3.53	-0.401	-	-	1.83	3.46	0.131 ^{ns}
CCE	%	12.5	70.6	45.7	25.3	Moderate	-0.365	0.375	0.098 ^{ns}
SOM	%	0.170	4.26	1.74	56.8	High	0.733	-0.055	0.104 ^{ns}

†: ns demonstrate no significant difference with the normal distribution and * indicates significant difference with the normal distribution at the probability level of 5%.

https://doi.org/10.1371/journal.pone.0296933.t003

Furthermore, the Kolmogorov-Smirnov test of normality showed the Na^+, EC, SAR, K^+, Mg^{2+}, and Ca^{2+} departed from normal distribution (Table 3). Normal distribution of the input data is an essential assumption for applying the MLR modeling procedure. There are different types of data transformations, like taking logarithm or natural logarithm, square rooting, squaring, etc. Therefore, the mentioned chemical attributes were transformed using the natural logarithm (ln or logarithm to the base e) function for being closer to the normal distribution.

Correlation between studied attributes

The Pearson's correlation coefficients (R) between the soil attributes are shown in Fig 3. As it was expected, the PSD-related parameters (i.e., silt, sand, σ_g, and d_g) and CCE had fair to relatively strong correlations with K_{15} and K_{10}. It means that among the studied different soil physico-chemical attributes, the PSD-related parameters are more significant for predicting K_{15} and K_{10}. Alternatively, by closing to saturation conditions, the soil structure-related parameters exhibited stronger correlations with K_ψ, in which K_5 and K_0 were significantly related to SOM, pH, CCE, BD, and ln(SAR). Therefore, it can be concluded that with increasing tension (i.e., decreasing matric potential), the variation of unsaturated hydraulic conductivity can be

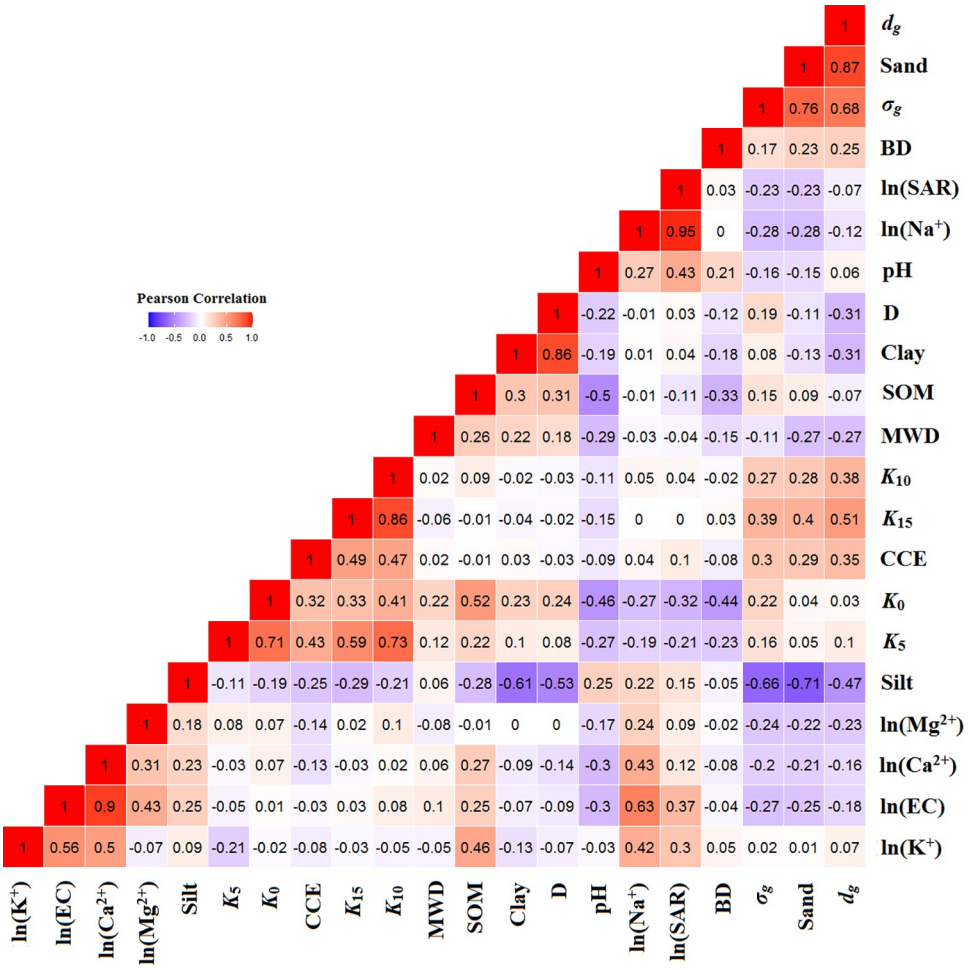

Fig 3. Pearson's correlation coefficients (R) among studied soil attributes.

https://doi.org/10.1371/journal.pone.0296933.g003

better described by soil PSD-related parameters compared to the soil structure-related parameters. To the best of our knowledge, with decreasing tension from 15 to 0 cm the dependency of water flow to macropores increases. Therefore, soil structure strongly affects the K_ψ values. Simultaneously, the pores size distribution changes with soil structure [81]. In the well aggregated and structured soils, high amounts of macropores exist due to large aggregates. Therefore, it is expected that all factors that affect soil structure have a significant influence on K_0 and to a lesser extent K_5. As we respected, the K_5 and K_0 were more sensitive to variations of SOM, pH, BD, and ln(SAR). By increasing tension from 0 to 15 cm, the diameter of pores contributed in water flow, and consequently the effects of macropores on water flow decreased. At high tensions (like 10 and 15 cm in the present study), the soil primary particles are placed next to each other within aggregates, and different mesopores and micropores are formed. Therefore, dependencies of K_{10} and K_{15} to the PSD-related parameters were remarkably increased.

Tajik et al. [82] confirmed that soil particles can be dispersed and soil structure can be destroyed in response to high amounts of Na^+ (SAR values), due to large hydrated radius. In addition, lower BD values might indicate more macropores in soils due to lower compaction. According to Vaezi et al. [83], Ostovari et al. [84,85], and Mozaffari et al. [86], the SOM and Ca^{2+} (represented by a high CCE) function as agents that bind mineral colloids together in

order to facilitate flocculation. This process leads to the formation and stability improvement of aggregates. In accordance with our results, Kotlar et al. [13], in different Danish soil types, observed that log(K_{10}) was powerfully related to PSD components (i.e., clay, sand, and silt contents) and the effects of these PSD parameters on log(K_0) decreased, while the impact of BD (structure-related parameter) increased. A significant correlation between clay and SOM contents and the values of ln(K_0) and ln(K_1) was found by Yang et al. [87]. Further, they reported ln(K_5) and ln(K_{10}) significantly related to MWD. Santra et al. [88] reported the ln(K_0) was significantly correlated with sand and clay contents, and BD in soils of Orissa, India.

Generally, the R values help us to clearly understand how each physico-chemical attribute is related to K_ψ. In addition, the appeared parameters in the developed SMLR-PTFs for predicting K_ψ at each applied tension are justified by R values. It should be noted that some physico-chemical attributes have collinearity, and therefore the more effective ones would appear in the SMLR-PTFs for predicting K_ψ.

Predicting K_ψ by SMLR method

The *t*-test analysis revealed that there were no statistically significant differences between the mean values of validation and calibration K_ψ across all applied tensions. In addition, the distributions of K_ψ values at all applied tensions in the mentioned subsets were relatively similar. Considering these conditions, we ensure that the data included in the validation subset are not concentrated in a specific small range of all data. Therefore, the validation subset can surely examine the developed models by the calibration subset. The developed PTFs using studied physico-chemical attributes by applying SMLR approach for predicting K_ψ are provided in Table 4. It is worth mentioning that, for predicting K_ψ, all studied soil physico-chemical attributes were imported to SMLR models as independent variables. The developed PTF for predicting K_{15} (Eq 20) using d_g, σ_g, silt, and CCE had R^2_{val} (subscript val shows validation subset), $NRMSE_{val}$ (%), NS_{val}, and RPD_{val} values of 0.55, 27.4, 0.52, and 1.47, respectively. In addition to these mentioned easily measurable soil attributes, the ln(SAR) was appeared to PTF developed for predicting K_{10} (Eq 21). The K_{10}-PTF predicted this property by R^2_{val}, $NRMSE_{val}$ (%), NS_{val}, and RPD_{val} values of 0.52, 25.9, 0.47, and 1.40, respectively. According to literature [89,90], the PSD and its related parameters can directly affect K_ψ at all tensions. For predicting K_5 and K_0, the silt, σ_g, SOM, and CCE were appeared with positive sign, while the ln(SAR) was introduced with a negative sign in the PTFs developed (Eqs 22 and 23). Furthermore, to predict K_0, the BD and pH contents were the influential factors by negative sign. By closing to saturated conditions, the macropores dependency of hydraulic conductivity increases [81]. Although the ln(Na^+) showed a significant correlation with both K_5 and K_0, the impact of ln (SAR) was more pronounced (Fig 3). The R^2_{val}, $NRMSE_{val}$ (%), NS_{val}, and RPD_{val} values were 0.56, 18.1, 0.49, and 1.44 for K_5 and 0.63, 25.4, 0.57, and 1.56 for K_0 predictions, respectively.

Table 4. Developed PTFs for predicting K_ψ using easily measurable soil attributes by applying the SMLR method.

$^{\dagger}K_{15} = -0.357 + 0.012(d_g) + 0.044(\sigma_g) + 0.003(\text{Silt}) + 0.005(\text{CCE})$	(20)
$K_{10} = -0.678 + 0.012(d_g) + 0.071(\sigma_g) + 0.008(\text{Silt}) + 0.008(\text{CCE}) - 0.068[ln(\text{SAR})]$	(21)
$K_5 = -0.781 + 0.085(\sigma_g) + 0.012(\text{Silt}) + 0.025(\text{CCE}) - 0.17[\ln(\text{SAR})] + 0.24(\text{SOM})$	(22)
$K_0 = 7.34 + 0.299(\sigma_g) + 0.035(\text{Silt}) + 0.08(\text{CCE}) - 0.632[\ln(\text{SAR})] + 1.08(\text{SOM}) - 0.778(\text{pH}) - 3.77(\text{BD})$	(23)

†: The calculated performance criteria for PTFs developed to predict K_ψ were presented in Table 5 (the units of the presented parameters are the same as these mentioned in Table 3).

https://doi.org/10.1371/journal.pone.0296933.t004

The PTFs (Eqs 20, 21 and 23) predicted K_{15}, K_{10}, and K_0 by fair accuracy according to NRMSE (20–30%) and RPD (1.4–1.8) values. Furthermore, The K_5-PTF (Eq 22) had good and fair accuracy based on NRMSE and RPD classifications, respectively. In addition, according to NS classification, the K_ψ across all of the applied tensions were predicted with unsatisfactory accuracy ($NS_{val} < 0.65$).

Overall, in comparison with K_{15}, K_{10}, and K_5, the K_0 was estimated more accurately. The moderate performance of K_ψ-PTFs was anticipated due to the considerable variability of K_ψ even in soils with similar characteristics. This variability is greatly affected by the geometry of the pores, which contributes to the dependency of K_ψ to the mentioned factor [20]. Although we used some soil structure-related parameters in the present study, they are unable to fully capture the complexity of soil structure. Nevertheless, due to the challenging, time-consuming, and costly nature of measuring K_ψ [10], a model that provides even moderate prediction of this property can still be highly beneficial and valuable. In accordance with our results, in the western desert of Egypt, Gamie and De Smedt [12] discovered that the parameters related to soil structure (carbonate content, SAR, BD, and water content in saturated, field capacity, and wilting point conditions) exhibited stronger correlations with $\log(K_0)$ as compared to the soil texture-related attributes (clay and silt contents). In contrast, Azadmard et al. [14] reported PTFs with R^2 values of 0.17, 0.21, 0.14, 0.19, and 0.19 for prediction of K_{15}, K_{10}, K_5, K_2, and K_0, respectively based on MLR approach using easily measurable soil attributes. Kotlar et al. [13] estimated $\log(K_0)$ and $\log(K_{10})$ with R^2 of 0.26 and 0.65, respectively using the SMLR method. In general, based on the statistical indices employed in this study, the K_ψ values at ψ of 15, 10, 5, and 0 cm were reasonably predicted using easily measurable soil attributes and applying SMLR method. The developed SMLR-PTFs can undergo testing, and subsequently be applied in other areas with the same soils.

Predicting K_ψ by MLPNNs and RBFNNs methods

Table 5 summarized the performance of all applied approaches in the present study for predicting K_ψ, i.e., SMLR, MLPNNs, and RBFNNs. As it was mentioned before, the imported independent variables to MLPNNs and RBFNNs models for predicting K_ψ at different applied tensions were these which appeared at Eqs (20) to (23). Regarding capability of MLPNNs approach to predict K_ψ, the K_{15}, K_{10}, K_5, and K_0 were predicted by respectively R^2_{val} values of 0.71, 0.78, 0.82, and 0.80. According to NRMSE classification, the K_{15}, K_{10}, and K_0 were

Table 5. The performance criteria for predicting K_ψ using easily measurable soil attributes by applying the SMLR, MLPNNs, and RBFNNs approaches.

Model	Attribute	Calibration subset				Validation subset			
		R^2	NRMSE	NS	RPD	R^2	NRMSE	NS	RPD
SMLR-PTF	K_{15}	0.58	25.4	0.58	1.56	0.55	27.4	0.52	1.47
	K_{10}	0.53	24.9	0.52	1.45	0.52	25.9	0.47	1.40
	K_5	0.60	16.4	0.60	1.60	0.56	18.1	0.49	1.44
	K_0	0.67	24.2	0.67	1.75	0.63	25.4	0.57	1.56
MLPNNs	K_{15}	0.78	22.3	0.68	1.79	0.71	23.7	0.65	1.71
	K_{10}	0.81	18.3	0.70	1.85	0.78	23.6	0.66	1.76
	K_5	0.84	11.7	0.81	2.33	0.82	13.1	0.75	2.05
	K_0	0.82	18.4	0.80	2.26	0.80	21.3	0.74	2.00
RBFNNs	K_{15}	0.67	22.8	0.63	1.63	0.58	24.7	0.59	1.50
	K_{10}	0.78	19.6	0.70	1.74	0.62	24.3	0.48	1.62
	K_5	0.80	16.0	0.78	2.07	0.78	17.1	0.74	1.87
	K_0	0.80	19.8	0.76	2.05	0.77	22.5	0.73	1.63

https://doi.org/10.1371/journal.pone.0296933.t005

predicted fairly (20% < $NRMSE_{val}$ < 30%) and K_5 was predicted with good accuracy ($NRMSE_{val}$ = 13.1%). The NS_{val} values showed acceptable accuracy (0.65 < NS_{val} < 0.80) for K_ψ at all applied tensions and RPD_{val} values showed very good predictions of K_5 and K_0 (2.05 and 2, respectively) and fair predictions of K_{15} and K_{10} (1.71 and 1.76, respectively).

On the other hand, The RBFNNs predicted K_{15}, K_{10}, K_5, and K_0 with R^2_{val} values of 0.58, 0.62, 0.78, and 0.77, respectively. Similar to SMLR and MLPNNs approaches, the RBFNNs predicted K_5 with good and the other studied K_ψs with fair accuracy based on $NRMSE_{val}$ values. The NS_{val} values illustrated acceptable accuracy for K_5 and K_0 (NS_{val} values of 0.74 and 0.73, respectively) and unsatisfactory accuracy for K_{15} and K_{10} (NS_{val} < 0.65). Furthermore, based on RPD_{val} values, just K_5 was predicted with good accuracy (RPD_{val} = 1.87) while, the K_{15}, K_{10}, and K_0 were fairly predicted using mentioned ANNs approach.

Jian et al. [40] reported adjusted R^2 of 0.53 and 0.33 related to the calibration and validation subsets, respectively to predict K_2 by applying MLPNNs by 2 hidden layers (5 and 3 neurons for the first and second hidden layers) and using clay, silt, and sand contents as inputs. Merdun et al. [32] predicted K_0 by R^2 value of 0.52 using sand, silt, clay, BD, and pores with diameter > 30 μm, between 3–30 μm, and < 3 μm as input variables and cascade forward neural network. Ghanbarian-Alavijeh et al. [34] used one hidden layer MLPNNs to estimate K_0 of UNSODA database. They found the mentioned approach successfully predicted K_0 (with R^2 values > 0.90) using clay and sand contents, BD, effective porosity and van Genuchten retention model parameters (θ_r, α, and n) as input variables.

Comparing potentials of SMLR, MLPNNs, and RBFNNs approaches to predict K_ψ

Discovering the most powerful modeling approach for predicting hardly measurable soil attributes is very crucial in soil modeling studies. To the best of our knowledge, soil management practices are closely related to hardly measurable soil attributes. The limitations and difficulties for direct measurement of K_ψ lead soil scientists to investigate different modeling procedures and discover the most accurate ones to predict this important attribute. Therefore, it is beneficial to compare the potential of classical regression methods (like SMLR) with artificial intelligence algorithms (like MLPNNs and RBFNNs) to predict K_ψ at different tensions. Table 5 shows that the values of R^2, NS, and RPD of different applied approaches for predicting K_ψ across all ψ were ranked as MLPNNs > RBFNNs > SMLR-PTFs and values of NRMSE was ranked as MLPNNs < RBFNNs < SMLR-PTFs. In order to better comparison between the capabilities of different approaches to predict K_ψ, we provided the values of R^2_{val} in Fig 4. Although the SMLR method provided simple and easy to use PTFs to predict K_ψ by using easily measurable soil attributes, their application may be limited due to relatively low accuracy. Of course, it should be pointed out that, for a property like hydraulic conductivity, these SMLR-PTFs are valuable due to difficulties in measuring K_ψ and its high variability. While, the MLPNNs approach showed a high capability (R^2_{val} > 0.70) for prediction of K_ψ across all ψ. This could be attributed to the presence of non-linear relations among the soil hydraulic and physico-chemical attributes [14].

Fig 5 shows the scatter plots of predicted against the observed (measured) K_ψ values across all ψ using MLPNNs as the best predictor approach. As can be seen, the points are near to 1:1 line for both validation and calibration subsets. In accordance with our results, Moosavi et al. [24] in soils of Fars Province, Iran, stated the capability of different approaches to predict sorptivity coefficient could be ranked as MLPNNs > RBFNNs > MLR regarding their accuracies and computational times. Furthermore, Shams Emamzadeh et al. [91] in soils of Tehran Province, Iran, found MLPNNs predicted K_0 was more accurate than that of RBFNNs. While,

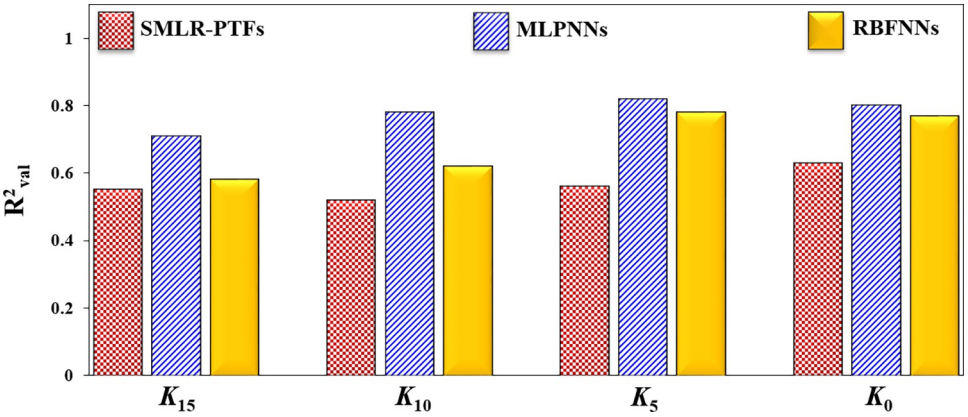

Fig 4. The column diagram of validation subset R^2 (R2val) values for predicting K_{15}, K_{10}, K_5, K_0 using easily measurable soil attributes by applying SMLR, MLPNNs, and RBFNNs approaches.

https://doi.org/10.1371/journal.pone.0296933.g004

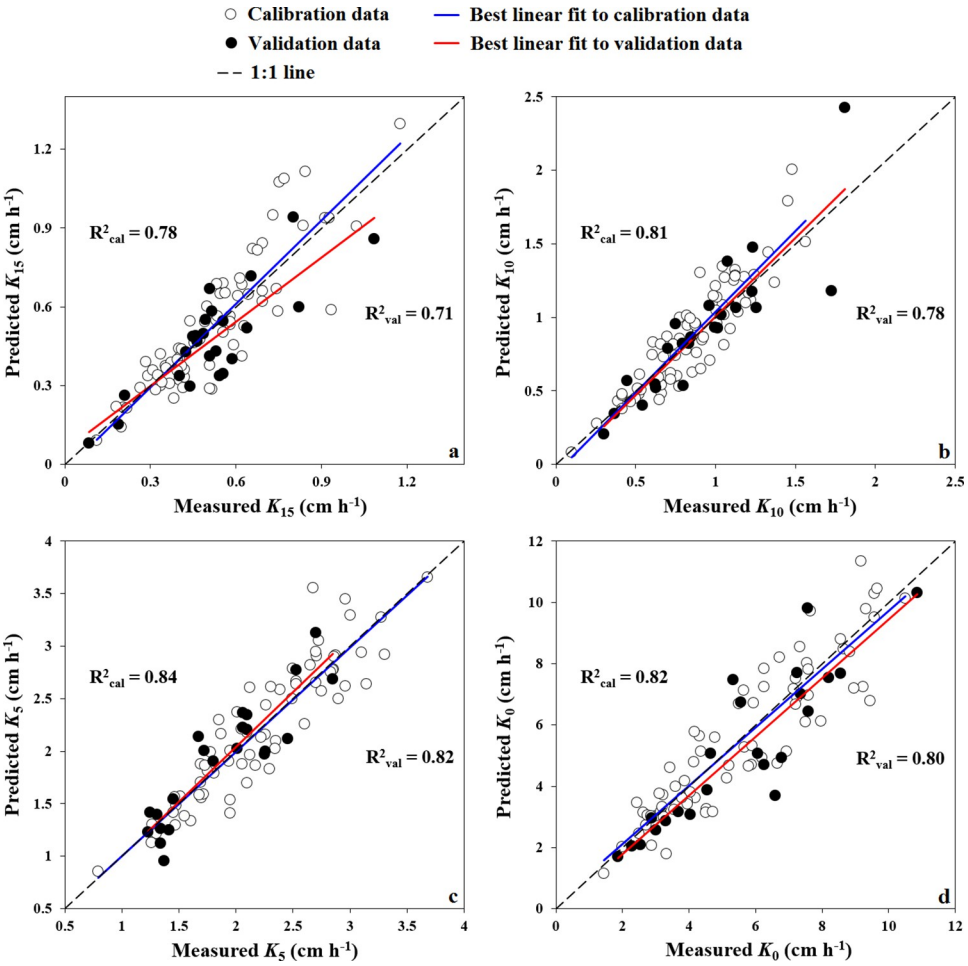

Fig 5. Scatter plots of the measured (observed) versus the predicted K_{15}, K_{10}, K_5, K_0 by applying MLPNNs approach as the best predictor and using easily measurable soil attributes.

https://doi.org/10.1371/journal.pone.0296933.g005

Rezaei Arshad et al. [36], reported more capability of RBFNNs to predict K_0 compared to MLPNNs and MLR methods in soils of Khuzestan Province, Iran. They predicted K_0 by R^2_{val} values of 0.68, 0.66, and 0.50 for RBFNNs, MLPNNs, and MLR approaches, respectively. Overall, the present study suggests using ANNs-based methods, especially MLPNNs, to predict saturated and near-saturated K_ψ. The proposed modeling approaches can be applied to predict hardly measurable soil attributes in different regions. Generally, the strengths of the present study were: i) obtaining relatively accurate to accurate predictions of saturated and near-saturated K_ψ in calcareous soils using MLPNNs, and ii) showing the high capability of artificial intelligence algorithms for modeling K_ψ compared to a classical regression approach (SMLR). However, other studies can be performed for testing other machine learning modeling procedures to predict soil-water-related parameters, especially K_ψ, and compare their potential with artificial intelligence algorithms. Furthermore, the developed SMLR-PTFs, can practically be tested in the same regions and then be used to predict K_ψ. For the ANNs-based approaches used, we suggest developing special MLPNNs and RBFNNs algorithms for predicting K_ψ by using easily measurable soil attributes in different areas.

Conclusions

The importance of K_ψ in water and chemical movements in the soil as well as the difficulties and time-consuming nature of its' measurement caused performing the present study aimed to investigate the potential of SMLR, MLPNNs, and RBFNNs approaches to predict K_ψ at 15, 10, 5, and 0 (saturated condition) cm tensions using easily measurable soil attributes in calcareous soils. According to Pearson's correlation coefficients, the PSD-related parameters were more correlated with K_{15} and K_{10} compared to structure-related parameters. The opposite results were obtained for K_5 and K_0. The MLPNNs approach provided the best prediction of K_ψ at all applied tensions by $0.71 \leq R^2_{val} \leq 0.82$ using recognized easily measurable soil attributes by SMLR-PTFs. In addition, the RBFNNs predicted K_ψ at all applied tensions acceptably to accurately with $0.58 \leq R^2_{val} \leq 0.78$. Although the developed SMLR-PTFs provided simple equations with relatively acceptable accuracy ($0.52 \leq R^2_{val} \leq 0.63$), the present study recommends ANNs-based approaches (specifically MLPNNs) to predict K_ψ at different tensions due to higher capability. Generally, the accuracy of K_ψ prediction at all applied tensions by using different approaches and easily measurable soil attributes was ranked as MLPNNs $>$ RBFNNs $>$ SMLR-PTFs. The K_ψ is a crucial factor in water resources management and in the field of soil science and it should be accurately determined in arid and semi-arid regions. The calcareous soils are normally placed in arid and semi-arid regions that face shortage of fresh water for agricultural activities. In addition, lime (calcium carbonate) can help aggregation, improve soil structure, and subsequently affect K_ψ in calcareous soils. The findings of the present study, especially the developed SMLR-PTFs, can practically be tested and then used in the other similar soils. Furthermore, the soils of different areas can benefit from the applied ANNs approaches to receive accurate predictions of K_ψ. Overall, machine learning algorithms (like those used in the present study) are beneficial for soil science researchers and professionals to find accurate PTFs for predicting and mapping the hardly measurable soil attributes in order to using in precision agriculture. For future works, we recommend paying more attention to predict soil hydraulic attributes in arid and semi-arid areas all over the world for using in water resources management and modeling the water and material transport within the soil. In addition, future studies can be performed to evaluate the performances of different machine learning approaches, like wavelet-neural networks, support vector regression, random forest, decision tree, cubist, k-nearest neighbors, etc. for predicting K_ψ. To conclude the present study, the readers should consider two important issues: i) accurate predictions of saturated

and near-saturated hydraulic conductivity in arid and semi-arid regions, and ii) application of powerful machine learning algorithms for accurate prediction of hardly measurable soil attributes.

Supporting information

S1 File. Highlights and Raw data are available as supplementary files.
(DOC)

S1 Raw data.
(XLS)

Acknowledgments

Authors appreciate financial supports of Shiraz University for carrying out the research. Authors also would like to thank dear Academic Editor, Prof. Dr. Al Mahfoodh and two esteemed anonymous Reviewers for the very constructive and valuable comments that really improved quality of the manuscript.

Author Contributions

Conceptualization: Ali Akbar Moosavi, Mohammad Amin Nematollahi.

Data curation: Hasan Mozaffari, Ali Akbar Moosavi, Mohammad Amin Nematollahi.

Formal analysis: Hasan Mozaffari, Ali Akbar Moosavi.

Funding acquisition: Ali Akbar Moosavi.

Investigation: Hasan Mozaffari, Ali Akbar Moosavi.

Methodology: Hasan Mozaffari, Ali Akbar Moosavi, Mohammad Amin Nematollahi.

Project administration: Ali Akbar Moosavi.

Resources: Ali Akbar Moosavi.

Software: Hasan Mozaffari, Ali Akbar Moosavi, Mohammad Amin Nematollahi.

Supervision: Ali Akbar Moosavi.

Validation: Hasan Mozaffari, Ali Akbar Moosavi, Mohammad Amin Nematollahi.

Visualization: Hasan Mozaffari, Ali Akbar Moosavi, Mohammad Amin Nematollahi.

Writing – original draft: Hasan Mozaffari, Ali Akbar Moosavi, Mohammad Amin Nematollahi.

Writing – review & editing: Hasan Mozaffari, Ali Akbar Moosavi, Mohammad Amin Nematollahi.

References

1. Verbist KMJ, Cornelis WM, Torfs S, Gabriels D. Comparing methods to determine hydraulic conductivities on stony soils. Soil Sci Soc Am J. 2013; 77: 25–42.
2. Rahmati M, Weihermüller L, Vanderborght J, Pachepsky YA, Mao L, Sadeghi SH, et al. Development and analysis of the Soil Water Infiltration Global database. Earth Syst Sci Data. 2018; 10: 1237–1263.
3. Bagarello V, Castellini M, Iovino M. Influence of the pressure head sequence on the soil hydraulic conductivity determined with tension infiltrometer. Appl Eng Agric. 2005; 21: 383–391.

4. Rogiers B, Mallants D, Batelaan O, Gedeon M, Huysmans M, Dassargues A. Estimation of hydraulic conductivity and its uncertainty from grain-size data using GLUE and artificial neural networks. Math Geosci. 2012; 44: 739–763.
5. Kodešová R, Jirků V, Kodeš V, Mühlhanselová M, Nikodem A, Žigová A. Soil structure and soil hydraulic properties of Haplic Luvisol used as arable land and grassland. Soil Tillage Res. 2011; 111: 154–161.
6. Villarreal R, Lozano LA, Salazar MP, Bellora GL, Melani EM, Polich N, et al. Pore system configuration and hydraulic properties. Temporal variation during the crop cycle in different soil types of Argentinean Pampas Region. Soil Tillage Res. 2020; 198: 104538.
7. Castellini M, Giglio L, Modugno F. Sampled soil volume effect on soil physical quality determination: A case study on conventional tillage and no-tillage of the soil under winter wheat. Soil Syst. 2020; 4: 72.
8. Nasta P, Romano N, Assouline S, Vrugt JA, Hopmans JW. Prediction of spatially variable unsaturated hydraulic conductivity using scaled particle-size distribution functions. Water Resour Res. 2013; 49: 4219–4229.
9. Dexter AR, Richard G, Arrouays D, Czyż EA, Jolivet C, Duval O. Complexed organic matter controls soil physical properties. Geoderma. 2008; 144: 620–627.
10. Vereecken H, Weynants M, Javaux M, Pachepsky Y, Schaap MG, van Genuchten MTh. Using pedotransfer functions to estimate the van Genuchten-Mualem soil hydraulic properties: A review. Vadose Zone J. 2010; 9: 795–820.
11. Sihag P, Tiwari NK, Ranjan S. Prediction of unsaturated hydraulic conductivity using adaptive neuro-fuzzy inference system (ANFIS). ISH J Hydraul Eng. 2017; 25: 132–142.
12. Gamie R, De Smedt F. Experimental and statistical study of saturated hydraulic conductivity and relations with other soil properties of a desert soil. Eur J Soil Sci. 2017; 69: 256–264.
13. Kotlar AM, Iversen BV, de Jong van Lier Q. Evaluation of parametric and nonparametric machine-learning techniques for prediction of saturated and near-saturated hydraulic conductivity. Vadose Zone J. 2019; 18: 180141.
14. Azadmard B, Mosaddeghi MR, Ayoubi S, Chavoshi E, Raoof M. Estimation of near-saturated soil hydraulic properties using hybrid genetic algorithm-artificial neural network. Ecohydrol Hydrobiol. 2020; 20: 437–449.
15. Mady AY, Shein EV. Support vector machine and nonlinear regression methods for estimating saturated hydraulic conductivity. Mosc. Univ. Soil Sci. Bull. 2018; 73: 129–133.
16. Sihag P, Mohsenzadeh Karimi S, Angelaki A. Random forest, M5P and regression analysis to estimate the field unsaturated hydraulic conductivity. Appl Water Sci. 2019; 9: 129.
17. Jorda H, Bechtold M, Jarvis N, Koestel J. Using boosted regression trees to explore key factors controlling saturated and near-saturated hydraulic conductivity. Eur. J. Soil Sci. 2015; 66: 744–756.
18. Tóth B, Weynants M, Nemes A, Mako A, Bilase G, Toth G. New generation of hydraulic pedotransfer functions for Europe. Eur. J. Soil Sci. 2015; 66: 226–238. https://doi.org/10.1111/ejss.12192 PMID: 25866465
19. Araya SN, Ghezzehei TA. Using machine learning for prediction of saturated hydraulic conductivity and its sensitivity to soil structural perturbations. Water Resour Res. 2019; 55: 5715–5737.
20. Van Looy K, Bouma J, Herbst M, Koestel J, Minasny B, Mishra U, et al. Pedotransfer functions in Earth system science: Challenges and perspectives. Rev Geophys. 2017; 55: 1199–1256.
21. Poznyak A, Chairez I, Poznyak T. A survey on artificial neural networks application for identification and control in environmental engineering: Biological and chemical systems with uncertain models. Annu Rev Control. 2019; 48: 250–272.
22. Zahedifar M. Assessing alteration of soil quality, degradation, and resistance indices under different land uses through network and factor analysis. Catena. 2023; 222: 106807.
23. Zahedifar M. Feasibility of fuzzy analytical hierarchy process (FAHP) and fuzzy TOPSIS methods to assess the most sensitive soil attributes against land use change. Environ Earth Sci. 2023; 82: 248.
24. Moosavi AA, Nematollahi MA, Rahimi M. Predicting water sorptivity coefficient in calcareous soils using a wavelet-neural network hybrid modeling approach. Environ Earth Sci. 2021; 80: 226.
25. Wang G, Wu J, Yin S, Yu L, Wang J. Comparison between BP neural network and multiple linear regression method. International Conference on Information Computing and Applications. Berlin, Heidelberg: Springer; 2010. pp 365–370.
26. Li QQ, Yue TX, Wang CQ, Zhang WJ, Yu Y, Li B, et al. Spatially distributed modeling of soil organic matter across China: an application of artificial neural network approach. Catena. 2013; 104: 210–218.
27. Soares dos Santos T, Mendes D, Rodrigues TR. Artificial neural networks and multiple linear regression model using principal components to estimate rainfall over South America. Nonlin Proc Geophys. 2016; 23: 13–20.

28. Cerny PA, Proximity MA. Data mining and neural networks from a commercial perspective. Orsnz conference twenty naught one. 2001; 1–10. https://api.semanticscholar.org/CorpusID:14690852.

29. Alsharif MH, Kelechi AH, Yahya K, Chaudhry SA. Machine learning algorithms for smart data analysis in internet of things environment: taxonomies and research trends. Symmetry. 2020; 12: 88.

30. Feng Y, Jia Y, Zhang Q, Gong D, Cui N. National-scale assessment of pan evaporation models across different climatic zones of China. J Hydrol. 2018; 564: 314–328.

31. Lu X, Ju Y, Wu L, Fan J, Zhang F, Li Z. Daily pan evaporation modeling from local and cross-station data using three tree-based machine learning models. J Hydrol. 2018; 566: 668–684.

32. Merdun H, Çınar Ö, Meral R, Apan M. Comparison of artificial neural network and regression pedotransfer functions for prediction of soil water retention and saturated hydraulic conductivity. Soil Tillage Res. 2006; 90: 108–116.

33. Baker L, Ellison D. Optimisation of pedotransfer functions using an artificial neural network ensemble method. Geoderma. 2008; 144: 212–224.

34. Ghanbarian-Alavijeh B, Liaghat AM, Sohrabi S. Estimating saturated hydraulic conductivity from soil physical properties using neural networks model. World Acad Eng Technol. 2010; 62: 131–136.

35. Motaghian H, Mohammadi J. Spatial estimation of saturated hydraulic conductivity from terrain attributes using regression, kriging, and artificial neural networks. Pedosphere. 2011; 21: 170–177.

36. Rezaei Arshad R, Sayyad G, Mosaddeghi M, Gharabaghi B. Predicting saturated hydraulic conductivity by artificial intelligence and regression models. Int Sch Res notices. 2013; 2013: 308159.

37. Sedaghat A, Bayat H, Sinegani AS. Estimation of soil saturated hydraulic conductivity by artificial neural networks ensemble in smectitic soils. Eurasian J. Soil Sci. 2016; 49: 347–357.

38. Moosavi AA, Sepaskhah AR. Artificial neural networks for predicting unsaturated soil hydraulic characteristics at different applied tensions. Arch Agron Soil Sci. 2012; 58: 125–153.

39. Sihag P. Prediction of unsaturated hydraulic conductivity using fuzzy logic and artificial neural network. Model Earth Syst Environ. 2018; 4: 189–198.

40. Jian J, Shiklomanov A, Shuster WD, Stewart RD. Predicting near-saturated hydraulic conductivity in urban soils. J. Hydrol. 2021; 595: 126051.

41. Beck HE. Zimmermann NE, McVicar TR, Vergopolan N, Berg A, Wood EF. Present and future Köppen-Geiger climate classification maps at 1-km resolution. Sci. Data. 2018; 5: 180214.

42. Gandomkar A, Dehghani R. 'Study of Temperature Changes in Fars Province'. World Acad Sci Eng Technol, Open Science Index 63, Int J Environ Eng. 2012; 6: 127–129.

43. MPB (Ministry of Programming and Budgeting). Economic and Social Status of Fars Province. Publication Centre for Informatics and Development Studies; 1994 (In Persian).

44. Khormali F, Abtahi A. Origin and distribution of clay minerals in calcareous arid and semi-arid soils of Fars Province, southern Iran. Clay Miner. 2003; 38: 511–527.

45. Banaei MH. Soil moisture and temperature regime map of Iran. Tehran, Iran: Soil and Water Research Institute, Ministry of Agriculture; 1998.

46. Ostovari Y, Moosavi AA, Mozaffari H, Poppiel RR, Tayebi M, Demattê JAM. Chapter 32-Soil erodibility and its influential factors in the Middle East. In: Pourghasemi HR, editor. Computers in Earth and Environmental Sciences. Elsevier; 2022. pp. 441–454.

47. Soil Survey Staff. Keys to Soil Taxonomy. 12th ed. Washington, DC: USDA-Natural Resource Conservation Service; 2014.

48. Gee GW, Bauder JW. Particle size analysis. In: Klute A, editor. Methods of Soil Analysis, Part 1, Physical and Mineralogical Methods. Madison, Wisconsin, USA: American Society of Agronomy and Soil Science Society of America; 1986. pp. 383–411.

49. Arshad MA, Lowery B, Grossman B. Physical tests for monitoring soil quality. In: Doran JW, Jones AJ, editors. Methods for Assessing Soil Quality. Madison, Wisconsin, USA; 1996. pp. 123–141.

50. Kemper WD, Rosenau RC. Aggregate stability and size distribution. In: Klute A, editor. Methods of Soil Analysis, Part 1, Physical and Mineralogical Methods. Madison, Wisconsin, USA: American Society of Agronomy and Soil Science Society of America; 1986. pp. 425–442.

51. Thomas GW. Soil pH and soil asidity. In: Sparks DL, Page AL, Helmke PA, Loeppert RH, Soltanpour PN, Tabatabai MA, Johnston CT, Sumner ME, editors. Methods of Soil Analysis, Part 3, Chemical and Microbiological Properties. Madison, Wisconsin, USA: American Society of Agronomy and Soil Science Society of America; 1996. pp. 475–490.

52. Nelson DW, Sommers LE. Total carbon, organic carbon, and organic matter. In: Sparks DL, Page AL, Helmke PA, Loeppert RH, Soltanpour PN, Tabatabai MA, Johnston CT, Sumner ME, editors. Methods of Soil Analysis, Part 3, Chemical and Microbiological Properties. Madison, Wisconsin, USA: American Society of Agronomy and Soil Science Society of America; 1996. pp. 961–1010.

53. Loeppert RH, Suarez DL. Carbonate and gypsum. In: Sparks DL, Page AL, Helmke PA, Loeppert RH, Soltanpour PN, Tabatabai MA, Johnston CT, Sumner ME, editors. Methods of Soil Analysis, Part 3, Chemical and Microbiological Properties. Madison, Wisconsin, USA: American Society of Agronomy and Soil Science Society of America; 1996. pp. 437–474.

54. Rhoades JD. Salinity: Electrical conductivity and total dissolved salts. In: Sparks DL, Page AL, Helmke PA, Loeppert RH, Soltanpour PN, Tabatabai MA, Johnston CT, Sumner ME, editors. Methods of Soil Analysis, Part 3, Chemical and Microbiological Properties. Madison, Wisconsin, USA: American Society of Agronomy and Soil Science Society of America; 1996. pp. 417–436.

55. Helmke P, Sparks DL. Lithium, sodium, potassium, rubidium, and cesium. In: Sparks DL, Page AL, Helmke PA, Loeppert RH, Soltanpour PN, Tabatabai MA, Johnston CT, Sumner ME, editors. Methods of Soil Analysis, Part 3, Chemical and Microbiological Properties. Madison, Wisconsin, USA: American Society of Agronomy and Soil Science Society of America; 1996. pp. 551–574.

56. Richards LA. Diagnosis and improvement of saline and alkali soils. In: Richards LA, editor. U. S. Salinity Laboratory Staff, USDA Hand Book NO. 60. Washangton, DC, USA; 1954. 160 P.

57. Shirazi MA, Boersma L. A unifying quantitative analysis of soil texture. Soil Sci Soc Am J. 1984; 48: 142–147.

58. Tyler SW, Wheatcraft SW. Fractal scaling of soil particle-size distributions: analysis and limitations. Soil Sci Soc Am J. 1992; 56: 362–369.

59. Mozaffari H, Moosavi AA, Ostovari Y, Cornelis W. Comparing visible-near-infrared spectroscopy with classical regression pedotransfer functions for predicting near-saturated and saturated hydraulic conductivity of calcareous soils. J Hydrol. 2022; 613: 128412.

60. Angulo-Jaramillo R, Vandervaere JP, Roulier S, Thony JL, Gaudet JP, Vauclin M. Field measurement of soil surface hydraulic properties by disc and ring infiltrometers: A review and recent developments. Soil Tillage Res. 2000; 55: 1–29.

61. Ankeny MD, Ahmed M, Kaspar TC, Horton R. Simple field method for determining unsaturated hydraulic conductivity. Soil Sci Soc Am J. 1991; 55: 467–470.

62. Wooding R. Steady infiltration from a shallow circular pond. Water Resour Res. 1968; 4: 1259–1273.

63. Gardner W. Some steady-state solutions of the unsaturated moisture flow equation with application to evaporation from a water table. Soil Sci. 1958; 85: 228–232.

64. Simunek J, Angulo-Jaramillo R, Schaap MG, Vandervaere J, van Genuchten MTh. Using an inverse method to estimate the hydraulic properties of crusted soils from tension-disc infiltrometer data. Geoderma. 1998; 86: 61–81.

65. Philip JR. The theory of infiltration. Adv Hydrosci. 1969; 5: 215–296.

66. White I, Sully MJ. Macroscopic and microscopic capillary length and time scales from field infiltration. Water Resour Res. 1987; 23: 1514–1522.

67. Nematollahi MA, Moosavi Khaneghah A. Neural network prediction of friction coefficients of rosemary leaves. J Food Process Eng. 2019; 42: e13211.

68. Moody JE, Darken CJ. Fast learning in networks of locally tuned processing units. Neur Comput. 1989; 1: 281–294.

69. Nawar S, Mouazen AM. Comparison between random forests, artificial neural networks, and gradient boosted machines methods of on-line vis-NIR spectroscopy measurements of soil total nitrogen and total carbon. Sensors. 2017; 17: 2428. https://doi.org/10.3390/s17102428 PMID: 29064411

70. Rodrigues E, Gomes A, Gaspar AR, Antunes CH. Estimation of renewable energy and built environment-related variables using neural networks—A review. Renew Sust Energy Rev. 2018; 94: 959–988.

71. Mozaffari H, Moosavi AA, Ostovari Y, Nematollahi MA, Rezaei M. Developing spectrotransfer functions (STFs) to predict basic physical and chemical properties of calcareous soils. Geoderma. 2022; 428: 116174.

72. Mozaffari H, Moosavi AA, Cornelis W. Vis-NIR-spectroscopy-and loss-on-ignition-based functions to estimate organic matter content of calcareous soils. Arch Agron Soil Sci. 2023; 69: 962–980.

73. Bannayan M, Hoogenboom G. Using pattern recognition for estimating cultivar coefficients of a crop simulation model. Field Crops Res. 2009; 111: 290–302.

74. Ritter A, Muñoz-Carpena R. Performance evaluation of hydrological models: Statistical significance for reducing subjectivity in goodness-of-fit assessments. J. Hydrol. 2013; 480: 33–45.

75. Mouazen AM, Kuang B, De Baerdemaeker J, Ramon H. Comparison among principal component, partial least squares and back propagation neural network analyses for accuracy of measurement of selected soil properties with visible and near infrared spectroscopy. Geoderma. 2010; 158: 23–31.

76. Mozaffari H, Moosavi AA, Dematte JA. Estimating particle-size distribution from limited soil texture data: Introducing two new methods. Biosyst Eng. 2022; 216: 198–217.

77. Sepaskhah AR, Tafteh A. Pedotransfer function for estimation of soil-specific surface area using soil fractal dimension of improved particle-size distribution. Arch Agron Soil Sci. 2013; 59: 93–103.

78. Bodhinayake W, Si BC, Xiao C. New method for determining water-conducting macro- and mesoporosity from tension infiltrometer. Soil Sci Soc Am J. 2004; 68: 760–769.

79. Mozaffari H, Moosavi AA, Sepaskhah A, Cornelis W. Long-term effects of land use type and management on sorptivity, macroscopic capillary length and water-conducting porosity of calcareous soils. Arid Land Res Manag. 2022; 36: 371–397.

80. Wilding LG, Soil spatial variability: Its documentation, accommodation and implication to soil surveys. In: Nielsen DR, Bouma J, editors. Soil Spatial Variability Proceedings of a Workshop of the ISSS and the SSA. Wageningen, USA: Las Vegas PUDOC; 1985. pp. 166–187.

81. Mozaffari H, Moosavi AA, Sepaskhah AR. Land use-dependent variation of near-saturated and saturated hydraulic properties in calcareous soils. Environ Earth Sci. 2021; 80: 769.

82. Tajik F, Rahimi H, Pazira E. Effects of electrical conductivity and sodium adsorption ratio of water on aggregate stability in soils with different organic matter content. J Agric Sci Technol. 2003; 5: 67–75.

83. Vaezi AR, Sadeghi SH, Bahrami HA, Mahdian M. Spatial variability of soil erodibility factor (K) of the USLE in North West of Iran. J Agric Sci Technol. 2010; 12: 241–252.

84. Ostovari Y, Ghorbani-Dashtaki Sh, Bahrami HA, Naderi M, Dematte JAM, Kerry R. Modification of the USLE K-factor for soil erodibility assessment on calcareous soils in Iran. Geomorphology. 2016; 273: 385–395.

85. Ostovari Y, Ghorbani-Dashtakia Sh, Bahrami HA, Dematte AM, Arthurd E, Panagos P. Towards prediction of soil erodibility, SOM and $CaCO_3$ using laboratory Vis-NIR spectra: A case study in a semi-arid region of Iran. Geoderma. 2018; 314: 102–112.

86. Mozaffari H, Rezaei M, Ostovari Y. Soil sensitivity to wind and water erosion as affected by land use in southern Iran. Earth. 2021; 2: 287–302.

87. Yang Y, Wendroth O, Kreba S, Liu B. Estimating near-saturated soil hydraulic conductivity based on its scale-dependent relationships with soil properties. Vadose Zone J. 2019; 18: 180217.

88. Santra P, Sahoo RN, Das BS, Samal RN, Pattanaik AK, Gupta VK. Estimation of soil hydraulic properties using proximal spectral reflectance in visible, near-infrared, and shortwave-infrared (VIS–NIR–SWIR) region. Geoderma. 2009; 152: 338–349.

89. Wang J, François B, Lambert P. Equations for hydraulic conductivity estimation from particle size distribution: a dimensional analysis. Water Resour. Res. 2017; 53: 8127–8134.

90. Zhang Y, Schaap MG. Estimation of saturated hydraulic conductivity with pedotransfer functions: A review. J. Hydrol. 2019; 575: 1011–1030.

91. Shams Emamzadeh ES, Soltani J, Mashal M, Kalanaki M, Asadolahzadeh T. Performance evaluation of MLP and RBF neural networks to estimate the soil saturated hydraulic conductivity. Mod Appl Sci. 2017; 11: 1–12.